Journal of Industrial and Engineering Chemistry xxx (xxxx) xxx

Contents lists available at ScienceDirect

Journal of Industrial and Engineering Chemistry

journal homepage: www.elsevier.com/locate/jiec

Full Length Article

Tri-layer hydrogel scaffold supporting co-culture paracrine signaling for accelerated skin repair

Yeong Hwan Kim [a,1], Gyubok Lee [b,1], Dongwoo Kim [b], Young-Ju Jang [a], Sang Yoon Lee [a], Kangwon Lee [b,*], Suk Ho Bhang [a,*]

[a] School of Chemical Engineering, Sungkyunkwan University, Suwon 16419, Republic of Korea
[b] Department of Applied Bioengineering, Graduate School of Convergence Science and Technology, Seoul National University, Seoul 08826, Republic of Korea

ARTICLE INFO

Keywords:
ADSC
Alginate
Fibrin
HUVEC
Hydrogel
Polycaprolactone
Wound Healing

ABSTRACT

The clinical management of complex skin wounds still lacks biomaterials that provide mechanical stability, pro-angiogenic signaling, and rapid tissue integration in a single platform. We engineered a tri-layer scaffold consisting of electrospun polycaprolactone fibers for initial structural support, a fibrin hydrogel for cell adhesion, and an alginate shell that creates a mildly hypoxic, nutrient-permissive niche. Co-seeding the scaffold with adipose-derived stem cells (ADSCs) and human umbilical vein endothelial cells (HUVECs) maintained high cell viability, strengthened paracrine crosstalk, and up-regulated genes involved in extracellular-matrix remodeling and angiogenesis in vitro. In a mouse dorsal-wound model the cell-laden construct accelerated closure, rebuilt a well-stratified epidermis and dermis, and generated dense microvascular networks compared with scaffold-only and single-cell controls. Histology confirmed organized collagen deposition with strong laminin and involucrin expression, indicating mature skin regeneration. The scaffold also displayed high swelling capacity, allowing it to conform to dynamic wound beds while managing exudate. These results show that a mechanically tuned tri-layer scaffold integrated with stem–endothelial co-culture can coordinate angiogenesis and tissue repair, supporting its potential for treating difficult cutaneous wounds.

Introduction

Skin is the body's largest organ, accounting for nearly one seventh of total body weight, and serves as a biochemical and mechanical barrier against microbes, trauma, and chemical irritation [1]. When this barrier is breached, a finely tuned sequence of hemostasis, inflammation, proliferation, and remodeling normally restores tissue structure and function [2]. If treatment is not appropriate, the cascade stalls in the inflammatory phase [3]. Biofilm-induced neutrophil activation raises reactive oxygen species and matrix metalloproteinases, degrades collagen and fibronectin, disrupts integrin signaling, and consequently drives DNA-damage senescence in resident fibroblasts and keratinocytes [4,5]. Non-healing ulcers worsen the clinical burden because they prolong hospital stays, markedly increase the risk of limb amputation, and elevate mortality [6]. Effective care must therefore rebuild healthy tissue rather than simply cover the wound [7].

First-line dressings such as hydrocolloid patches, polymer films, and antiseptic ointments help balance moisture, provide a physical barrier, and limit bacterial growth, yet they still fail in key respects [8]. Adhesives lose cohesion under sweat or heavy exudate, films peel from highly mobile sites such as ankles and elbows, and topical antibiotics or steroids can trigger dermatitis or systemic effects [9,10,11]. Even the advanced exudate-absorbing foams provide moisture control but do little to enhance vascular ingrowth or support extracellular-matrix remodeling [12]. Accordingly, next-generation dressings need to combine mechanical support with precisely delivered biochemical and cellular cues to restart the healing program [13].

Cell-based approaches address this need by supplying a living source of trophic factors [14]. Adipose-derived stem cells are abundant, can be harvested under local anesthesia, and show low immunogenicity [15]. They secrete vascular endothelial growth factor, hepatocyte growth factor, and basic fibroblast growth factor, which recruit fibroblasts, stimulate keratinocyte migration, and guide macrophages toward a pro-repair phenotype [16]. Human umbilical vein endothelial cells

* Corresponding authors at: Department of Applied Bioengineering, Graduate School of Convergence Science and Technology, Seoul National University, Seoul 08826, Republic of Korea, School of Chemical Engineering, Sungkyunkwan University, Suwon 16419, Republic of Korea.
E-mail addresses: kangwonlee@snu.ac.kr (K. Lee), sukhobhang@skku.edu (S.H. Bhang).
[1] **Co-first authors**: These authors contributed equally to this work.

https://doi.org/10.1016/j.jiec.2025.08.021
Received 27 May 2025; Received in revised form 18 July 2025; Accepted 9 August 2025
Available online 10 August 2025

spontaneously form branched tubules, release angiopoietin-2 and nitric-oxide modulators, and accelerate inosculation with host microvasculature [17]. When cultured together the two cell types support each other's survival, amplify paracrine signaling, and generate pre-vascular networks that outperform monocultures in animal models [18,19]. However, clinical translation is still limited by three barriers, namely poor cell retention in the wound, rapid loss of viability in the exudate, and loss of local cytokine gradients [20].

These challenges make scaffold design pivotal to successful wound healing [21]. An ideal construct should match the tensile and compressive moduli of skin, withstand suturing and flexion, present adhesive ligands for rapid cell anchorage, and regulate moisture and oxygen [22]. Electrospun polycaprolactone nanofibers provide skin-like elasticity, aligned contact-guidance cues, and strong clinical safety [23]. Fibrin hydrogel replicates the provisional matrix formed during hemostasis, supplies RGD sites for integrin binding, and degrades enzymatically to support remodeling [24]. Ionically cross-linked alginate offers high water uptake, adjustable stiffness, and a mildly hypoxic niche that elevates HIF-1α and vascular endothelial growth factor expression in embedded cells [25].

Although polycaprolactone, fibrin, and alginate have each been used on their own, their combined potential in a hierarchical construct remains underexplored [26]. A tri-layer configuration can address long-standing design conflicts. A polycaprolactone core seeded with adipose-derived stem cells provides structural support and secures the hydrogel layers [27]. A fibrin middle layer seeded with human umbilical vein endothelial cells recreates early granulation tissue and promotes matrix remodeling [28]. An alginate shell absorbs exudate, maintains a moist environment, and protects the endothelial network while its controlled hypoxia enhances angiogenic signaling [29]. Spatial arrangement of the two cell types stabilizes heterotypic contacts, strengthens reciprocal paracrine feedback, and encourages rapid inosculation with host vessels as alginate pores enlarge during ion exchange [30].

In this study we fabricate a tri-layer (polycaprolactone, fibrin, alginate) scaffold designed to harness adipose-derived stem cell and human umbilical vein endothelial cell synergy for rapid skin regeneration. Electrospinning and hydrogel parameters are tuned to match native dermal mechanics, and swelling assays confirm effective exudate management. After verifying biocompatibility we assess cell proliferation, resistance to oxidative stress, and expression of genes involved in extracellular-matrix remodeling and angiogenesis. We also evaluate whether the alginate shell forms a hypoxia gradient that increases vascular growth-factor release without inducing necrosis. Therapeutic performance is evaluated in a mouse dorsal wound model that measures closure rate, collagen architecture, epidermal stratification, basement-membrane restoration, and microvessel protein density. Scaffolds without cells and single-cell controls help isolate the effects of architecture and co-culture. By combining skin-level mechanics, cell-adhesive cues, exudate control, and oxygen-modulated paracrine amplification in a single construct, we present a versatile platform that addresses persistent shortcomings in wound therapy and can be adapted to diabetic ulcers, radiation injuries, and large donor-site defects.

Materials and methods

Cell culture

Human adipose-derived stem cells (ADSC), isolated from adipose tissue obtained from healthy adult donor (female) were purchased from Lonza (Basel, Switzerland) and cultured in Dulbecco's Modified Eagle's Medium (DMEM; Gibco BRL, MD, USA) supplemented with 10 % (v/v) fetal bovine serum (FBS; Cellsera, Australia) and 1 % (v/v) penicillin/streptomycin (PS, Welgene, Daegu, Republic of Korea). Human umbilical-vein endothelial cells (HUVEC), isolated from the vein of the umbilical cord from newborn (female) were purchased from Lonza and cultured in endothelial basal medium-2 (Lonza) supplemented with endothelial growth supplement single Quots (Lonza) and 1 % (v/v) PS (Welgene). The cells were incubated at 37 °C with 5 % CO_2 saturation. The cell culture medium was changed every 2 days. Cells within over 3 passages were used in the experiments.

Scaffold fabrication

Poly(ε-caprolactone) (PCL, $M_n \approx 80$ kDa; Sigma-Aldrich) was dissolved at 20 % w/v in 2,2,2-trifluoroethanol and electrospun for 30 min. The polymer solution was delivered through an 18-gauge stainless-steel needle at 0.8 mL h^{-1} while a 7.5 kV potential difference was applied between the spinneret and a grounded aluminum collector. The non-woven mat obtained was punch-cut into 5 mm squares and sterilized in 70 % ethanol. Each PCL square was transferred to a 96-well plate and seeded with human adipose-derived stem cells (ADSC, 1.25×10^5 cells per scaffold) suspended in 20 μL Dulbecco's modified Eagle medium (DMEM). After a 30 min incubation at 37 °C in 5 % CO_2, a fibrin layer containing human umbilical-vein endothelial cells (HUVECs) formed directly on the fibre mesh. For this step, HUVECs (2.5×10^5 cells) were dispersed in 80 μL fibrinogen solution (20 mg mL^{-1} in 3 % w/v NaCl), mixed with 8 μL thrombin (2.5 U mL^{-1} in 20 mM $CaCl_2$), and allowed to gel for 30 min at 37 °C. The resulting PCL–fibrin composite was carefully lifted with a sterile micro-spatula and immersed in 5 mL of 1 % w/v sodium alginate solution contained in a six-well plate. Immediate ionic cross-linking was initiated by gently layering 5 mL of 1 % w/v $CaCl_2$ onto the bath for 30 s at room temperature, producing a thin alginate envelope around the fibrin core. Finished constructs were rinsed twice in phosphate-buffered saline and stored in complete culture medium until further use. The seeding densities were 2.6×10^6 and 5.1×10^6 cells cm^{-3} for ADSCs and HUVECs, respectively.

Visualization and analysis of the scaffold via CCD camera and electron microscopy

For the visualization and analysis of the scaffold, we employed the CCD camera integrated into the iPhone 13. The scaffold was positioned and carefully aligned, ensuring that it was approximately 10 cm away from the camera lens during the capturing process. Scanning electron microscopy (SEM; Helios 5 UC, Thermo Fisher Scientific, MA, USA) was used to analyze the external structures of the scaffold. Before the analysis, the scaffolds were coated with a layer of platinum through a sputter-coating process. The SEM investigation was conducted under an acceleration voltage set to 10 kV, ensuring high-resolution imagery and detailed insight into the surface topography of the scaffold.

Evaluating the mechanical property of the scaffold

To evaluate the mechanical characteristics of the tri-layer scaffolds, assessments were conducted on the compressive modulus of the fibrin hydrogel, PCL-fibrin hybrid scaffold, and the tri-layer scaffolds themselves. These evaluations were conducted using an Instron 3343 testing machine (Instron, MA, USA). Initially, each scaffold was submerged in phosphate buffered saline (PBS; Welgene, South Korea) allowing it to undergo swelling for 30 mins. Surplus or remaining fluid was diligently removed to prepare for the forthcoming analysis. The scaffolds were then placed on the machine and subjected to a compressive force. Throughout the process, both the compressive stress and compressive strain exerted on the scaffolds were meticulously recorded. Utilizing the data gathered from these measurements, calculations were made to determine the true stress and strain values. The viscoelastic properties of the scaffolds were thoroughly analyzed using a dynamic shear modulus deformation approach. The specimens were carefully positioned between a metal plate measuring 2 cm, with a gap of 1 cm maintained between them. A rheometer (MCR 102, Anton Paar, Graz, Australia) was

employed to evaluate their vibration-shear deformation. To determine the storage modulus of the samples, they were subjected to continuous deformation mode. Throughout this process, a consistent strain of 10 % was applied across a frequency range of 0.1 to 300 Hz (rad/s), all conducted at a controlled temperature of 25 °C. The swelling capacity of the hydrogel samples was assessed by recording changes in their weight at various intervals, with all measurements taken at 37 °C. Before the swelling test, the hydrogel samples were dried at 70 °C oven overnight and then rehydrated in PBS buffer. To ensure accuracy in our measurements, any excess PBS present on the surface of the hydrogel was delicately absorbed using filter paper, and the samples were then weighed three times to obtain reliable data. The swelling ratio of the hydrogels was calculated utilizing the formula $(W_t - W_0)/W_0 \times 100$ %, where W_t represents the weight of the swollen hydrogel at a specific time, and W_0 denotes its initial dry weight. This calculation provided a quantitative measure of the hydrogel's ability to absorb and retain fluid, an important parameter in understanding its swelling performance characteristics. To investigate hydrogel stability, hydrogels were monitored for mass loss over a 10-day immersion in phosphate-buffered saline (PBS, Welgene) maintained at 37 °C. Hydrogels were fully submerged in PBS. Each day, samples were retrieved, lightly rolled on lint free tissue to remove surface moisture, and weighed immediately. Daily measurements were recorded for all samples across the 10-day period to quantify relative weight retention.

Cell viability test

To evaluate the biocompatibility of the hydrogel composite, an indirect cytotoxicity assessment was performed on ADSCs and HUVECs according to the international standard (ISO 10993–12). Initially, extracts of the hydrogel composite were prepared by immersing the material in a serum-free medium at a density of 200 mg/mL and allowing it to incubate for 2 days at 37 °C. Calcein AM and EthD-1 staining was conducted to observe live and dead signals from ADSCs and HUVECs after hydrogel extracts treatment. Briefly, ADSCs and HUVECs seeded in 24-well plates (5×10^4 cells/well) were treated with hydrogel extracts (200 mg/mL) for 1, 4, and 7 days. After washing with PBS, the cells were incubated with a solution containing 2 μM Calcein AM and 4 μM EthD-1 for 30 min at room temperature. A laser scanning microscope from Carl Zeiss (Oberkochen, Germany) was utilized for image capture and analysis. To further assess the compatibility of cells with the hydrogel scaffolds directly, each cell type (ADSC and HUVEC) was cultured within the hydrogel matrices for a week. Post-incubation, a similar staining procedure was applied using Calcein AM and EthD-1 to facilitate the visualization of live and dead cells, respectively by using a laser scanning microscope from Carl Zeiss. The resulting fluorescence images were acquired to ascertain cellular behavior within the hydrogel environment. Z-stack series were collected through the full hydrogel and reconstructed to visualize the three-dimensional distribution of live and dead cells.

Cell proliferation test

The in vitro cell proliferation studies over the tri-layer scaffolds were conducted by EZ-Cytox (DoGenBio, Seoul, Korea). In brief, hydrogel extracts were prepared by swelling the scaffold composite in the media containing 10 % FBS serum at a concentration of 0.2 g/mL in an incubator for 48 h at 37 °C. Scaffold types were sterilized in 0.1 % (v/v) peracetic acid (Sigma-Aldrich) and scaffolds were rinsed in sterile PBS for 3 h. ADSCs and HUVECs were seeded at a density of 5×10^4 cells per well on 24-well plates for 48 h. After treating the cells with hydrogel extract solution in the same manner as described above, the cell proliferation at 1, 4, and 7 days was observed by adding MTT assay solution for 30 min, and the absorbance was measured at 450 nm using a microplate reader (Synergy H1, BioTek, VT, USA).

Quantitative reverse transcription-polymerase chain reaction (qRT-PCR) analysis

Total ribonucleic acid (RNA) was extracted from the samples using 1 mL of TRIzol (Invitrogen, CA, USA) and 200 μL of chloroform (Sigma-Aldrich). The samples were centrifuged for 10 min at 12,000 rpm at 4 °C. The RNA pellet was washed with 75 % (v/v) ethanol (Sigma-Aldrich) in water, after which it was dried. Afterward, the samples were dissolved in ribonuclease (RNase)-free water (iNtRON Biotechnology, Seoul, Korea). Further, reverse transcription was performed using 1.5 μg of pure total RNA and PrimeScript RT Master Mix (TaKaRa, Kusatsu, Japan), followed by the PCR amplification of the synthesized complementary DNA (cDNA). For qRT-PCR, the SsoAdvanced™ Universal SYBR Green Supermix Kit (Bio-Rad, CA, USA) and the CFX Connect™ real-time PCR Detection System (Bio-Rad) were used. qRT-PCR was performed to quantify the relative expression levels of matrix metalloproteinase-1(MMP1), collagen type III (COL3), cluster of differentiation 31 (CD31), fibroblast growth factor 2 (FGF2), vascular endothelial growth factor receptor (VEGFR), connexin 37 (Cx37) and connexin 43 (Cx43). Glyceraldehyde 3-phosphate dehydrogenase (GAPDH) was used as an internal control. Primer sequences are listed in Table 1.

Cell migration assay

To perform the cell scratch migration assay, human fibroblasts (CCD-986 sk) were cultured in 6-well plates until they reached confluence. After the cells were exposed to red light, the cell monolayer was scratched with a sterile 200 μL tip (Neptune Scientific, CA, USA) to create a linear gap. The floating cells were removed by washing with PBS. After incubating for 1, 6, 12, and 24 h, the gap width of the scratch re-population was measured and compared to the initial gap size at 0 h. Using Adobe Photoshop CC (Adobe systems, CA, USA), the size of the denuded area was determined at each time point from digital images. The relative migration area (%) was calculated using the following formula: $(A_0\text{-}A_t)/A_0 \times 100$ %, where A_t represents the dimensions of the recovered area at a specific time, and A_0 denotes the dimensions of the initial area.

Wound treatment

200 μL xylazine (20 mg/kg) and ketamine (100 mg/kg) diluted in saline solution were used to anesthetize six-week-old female athymic mice (20–25 g body weight, Orient, Seoul, Korea). Surgery was

Table 1
Qrt-pcr primer sequences.

Gene	Primer Sequence (5́-3́)
Human *GAPDH*	Forward: GTC TCC TCT GAC TTC AAC AGC G
	Reverse: ACC ACC CTG TTG CTG TAG CCA A
Human *Col3*	Forward: ACA CGT TTG GTT TGG AGA GTC C
	Reverse: CTG CAC ATC AAC GAC ATC TTC AG
Human *MMP1*	Forward: AGT GAC TGG GAA ACC AGA TGC TGA
	Reverse: GCT CTT GGC AAA TCT GGC CTG TAA
Human *VEGFR*	Forward: CAC CAC TCA AAC GCT GAC ATG TA
	Reverse: GCT CGT TGG CGC ACT CTT
Human *FGF2*	Forward: AAC GGT TAG CAC ACA CTC CTT
	Reverse: CGA CCC TCA CAT CAA GCT ACA
Human *CD31*	Forward: CTC GTT GTT GGA GTT CAG AAG TGG
	Reverse: ATT GCA GTG GTT ATC ATC GGA GTG
Human *HIF-1α*	Forward: TAT GAG CCA GAA GAA CTT TTA GGC
	Reverse: CAC CTC TTT TGG CAA GCA TCC TG
Human *VEGF*	Forward: GAG ATG AGC TTC CTA CAG CAC
	Reverse: TCA CCG CCT CGG CTT GTC ACA T
Human Cx43	Forward: GGT GGG TAA GAT CTG GCT GA
	Reverse: GGT GGG TAA GAT CTG GCT GA
Human Cx37	Forward: TCT GAG TGC CTG AAC TTG C
	Reverse: ACT GAC AGC CAC ACC TTC C

performed to remove a square (4 cm^2) section of the dorsal skin. Eight 6–0 sutures (AILEE Co., Busan, Korea) were positioned at the edge of each wound following skin removal to stop skin contracture from causing the wound to collapse. Following skin wound modeling, the mice were split into four groups: No treatment (wounds covered with only commercial skin dressing, Tegaderm, 3 M Healthcare, St. Paul, MN, USA), Scaffold only (scaffold loaded on skin wound and covered with the Tegaderm), HUVEC + ADSC (HUVECs and ADSCs were loaded on skin wound and covered with the Tegaderm), and Scaffold + HUVEC + ADSC (HUVECs and ADSCs with the scaffold was loaded on skin wound and covered with the Tegaderm). The No treatment group was served as control group. All animals received care according to the Guidelines for the Care and Use of Laboratory Animals of Sungkyunkwan University (SKKUIACUC2023-06–17-2, June 2023).

Preparation of histological sample

Samples of skin tissue were collected ten days after the treatments and preserved using a 4 % formaldehyde solution. To create 10 μm sections, the samples were frozen after being embedded in an OCT compound (SciGen Scientific, Gardenas, CA, USA). Hematoxylin and eosin (H&E) staining and Masson's trichrome (MT) were performed to analyze the samples.

Immunohistochemistry

Tissue samples embedded in OCT compound were cryo-sectioned at a thickness of 10 μm at − 22°C. For immunohistochemical analysis of epithelialized regions, primary antibodies against CD31, laminin, and involucrin (Abcam, Cambridge, UK) were applied. Detection of CD31, laminin, and involucrin was achieved using fluorescein isothiocyanate (FITC)-conjugated secondary antibodies (Jackson ImmunoResearch Laboratories, West Grove, PA, USA). Nuclei were counterstained with 4′,6-diamidino-2-phenylindole (DAPI, Vector Laboratories, Burlingame, CA, USA), and the stained sections were visualized under a fluorescence microscope (DFC3000 G, Leica).

Statistical analysis

All quantitative results are expressed as mean ± standard deviation (SD). Statistical analyses were executed using GraphPad Prism (GraphPad Software, San Diego, CA, USA). Comparisons between two groups were assessed by an unpaired Student's *t*-test, and comparisons among three groups were analyzed using ordinary one-way ANOVA. A p-value is less than 0.05 was considered indicative of statistical significance.

Results

Characterization of the tri-layer hydrogel scaffold

The fabricated tri-layer scaffold exhibited robust structural stability, with each component contributing to its integrity. Macroscopic images showed that the outer alginate layer formed a translucent shell approximately 2 mm thick around the fibrin-PCL core, markedly improving the scaffold's shape retention compared to an uncoated fibrin hydrogel (Fig. 1a, Fig. S1). At the microscopic level, scanning electron microscopy revealed a porous fibrin matrix interlaced with stable PCL nanofiber strands (Fig. 1b).

The tri-layer construct's mechanical properties were characterized by rheometry and tensile testing. Dynamic rheology measurements indicated that pure fibrin hydrogel had the lowest storage (G′) and loss (G″) moduli, consistent with it being the softest formulation (Fig. 1c). Incorporating PCL nanofibers into fibrin increased both moduli to intermediate levels, whereas the full Fibrin + PCL + Alginate scaffold showed the highest G′ and G″ values. This trend demonstrates that each added component incrementally reinforces the scaffold's stiffness and viscoelasticity. Similarly, stress–strain testing revealed distinct mechanical behaviors for each composition (Fig. 1d). The fibrin-only scaffold exhibited the lowest stress at a given strain (reflecting its inherent softness), while the fibrin + PCL composite withstood higher stresses, indicating that PCL fibers fortify the network. Notably, the tri-layer hydrogel scaffold achieved the greatest stress values across all strains, underscoring the synergistic effect of combining these materials to produce a construct with superior mechanical robustness.

The swelling behavior of the scaffolds was also assessed (Fig. 1e–f). All formulations swelled substantially, but the tri-layer scaffold reached its equilibrium swelling ratio more rapidly than fibrin alone. The fibrin hydrogel demonstrated a high swelling ratio, whereas the Fibrin + PCL + Alginate scaffold not only equilibrated faster but ultimately attained the highest swelling ratio (exceeding 1000 % of its dry weight). This exceptional swelling capacity suggests that the tri-layer scaffold can effectively absorb large amounts of fluid, such as wound exudate, which is beneficial for maintaining a moist wound environment conducive to healing. An additional in-vitro mass loss study under physiological conditions was conducted (Fig. S2). The fibrin scaffold lost almost its entire mass within four days, reflecting rapid fibrin breakdown once the outer coating is absent, whereas the complete tri-layer hydrogel construct degraded gradually, retaining about fifty percent of its initial weight after ten days.

Cytocompatibility evaluation of the tri-layer hydrogel scaffold

The biocompatibility of the tri-layer hydrogel scaffold was confirmed through cell culture studies with adipose-derived stem cells and human umbilical vein endothelial cells. Live/dead fluorescence imaging of ADSCs cultured with scaffold extract and encapsulated in the scaffold over 7 days showed robust cell viability (Fig. 2a). At Day 1, cells exhibited intense green fluorescence (live cells) with negligible red fluorescence (dead cells). By day 4, a few red spots emerged, indicating minor cell death, but the overall signal remained predominantly green. this trend continued through day 7, demonstrating sustained cell survival in the scaffold microenvironment. Similarly, HUVECs cultured in the scaffold displayed no signs of apoptosis over 7 days and proliferated within the matrix (Fig. 2b), further indicating the construct's outstanding cytocompatibility. Additionally, 3D z-stack confocal live/dead imaging was conducted (Fig. S3). In all stacks, the scaffold center uniformly displayed green fluorescence with only isolated red signals, and quantitative analysis confirmed overall viability above 90 percent at each time point.

Cell proliferation assays corroborated these imaging results (Fig. 2c). After 1 day of culture, ADSCs showed a slightly higher proliferation rate than HUVECs, but by day 7 the proliferation of both cell types had increased and converged to similar levels. Neither cell type showed significant apoptotic signals during the incubation period. These observations confirm that the tri-layer scaffold supports the growth of both mesenchymal stem cells and endothelial cells, maintaining high viability and encouraging cell expansion over time.

qRT-PCR analysis after 3 days of 3D culture revealed that the scaffold environment also elicited a pro-healing genetic response. In the combined HUVEC + ADSC group, there was significant upregulation of extracellular matrix remodeling markers (collagen type III (COL3) and matrix metalloproteinase-1 (MMP1)) as well as angiogenic markers (vascular endothelial growth factor receptor (VEGFR), basic fibroblast growth factor (FGF2), and CD31) compared to cells cultured alone (Fig. 2d). In addition, expression of cell–cell interaction markers Cx43 and Cx37 was also increased in the HUVEC + ADSC group, suggesting improved intercellular communication within the tri-layer scaffold (Fig. 2e). These results suggest that the tri-layer scaffold provides a microenvironment that synergistically activates wound-healing pathways in the cells. The encapsulated cells likely experienced mild hypoxic conditions within the 3D matrix, as supported by the increased HIF-1α expression observed in scaffold cultures, which can activate the HIF-1α/

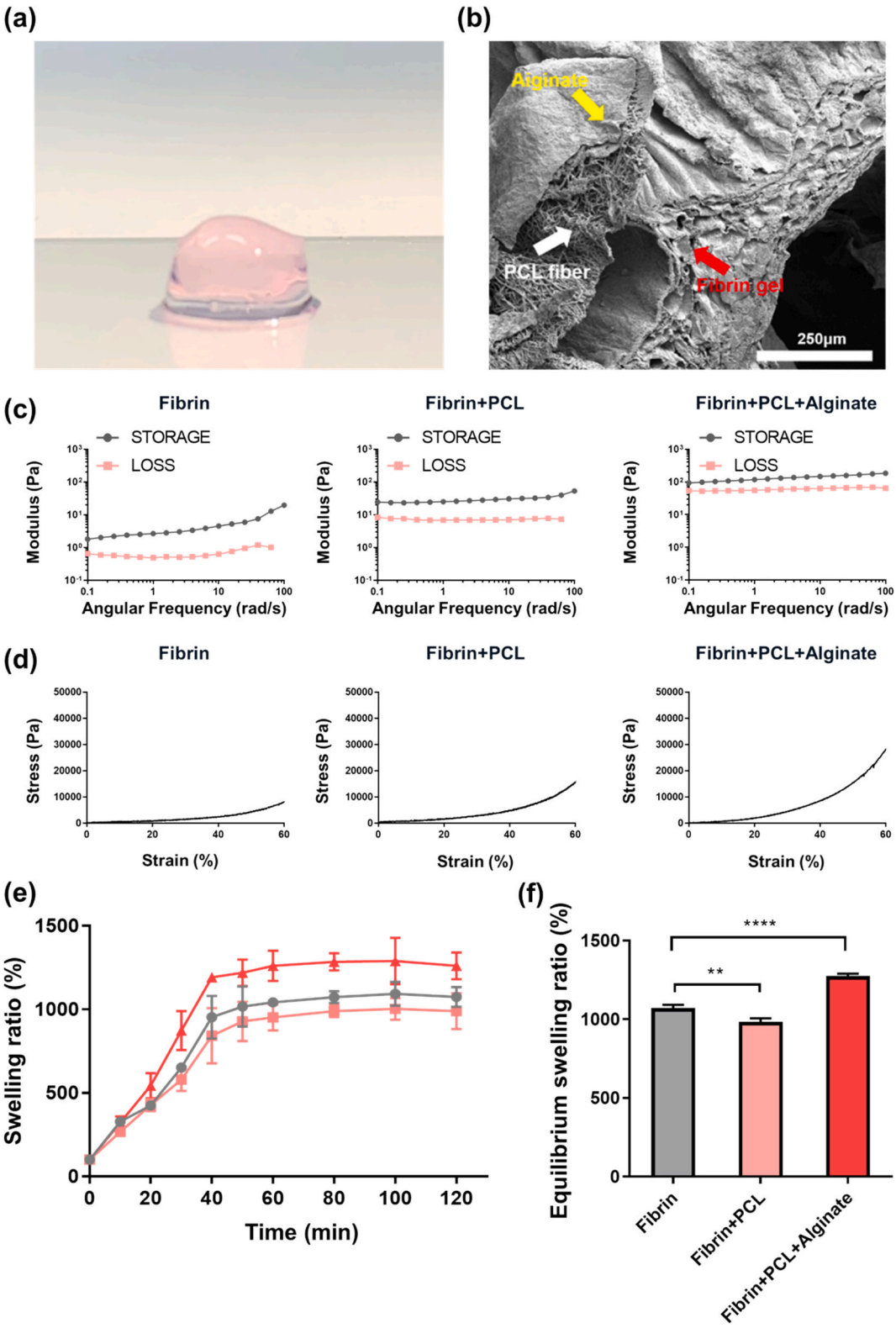

Fig. 1. Characterization of the tri-layer hydrogel scaffold for wound repair. **(a)** Macroscopic photographs of the tri-layer scaffold. **(b)** Characteristic SEM image revealing the layered structure of the Tri-layer hydrogel scaffold (Scale bar = 250 μm). **(c)** Dynamic rheology measurements (Storage and Loss modulus) of the scaffolds with different compositions. **(d)** Stress-Strain curve of the scaffolds with different compositions. **(e)** Time-dependent swelling kinetics (n = 3) and **(f)** corresponding equilibrium swelling ratios (n = 5, **p < 0.01, ****p < 0.0001 versus fibrin group).

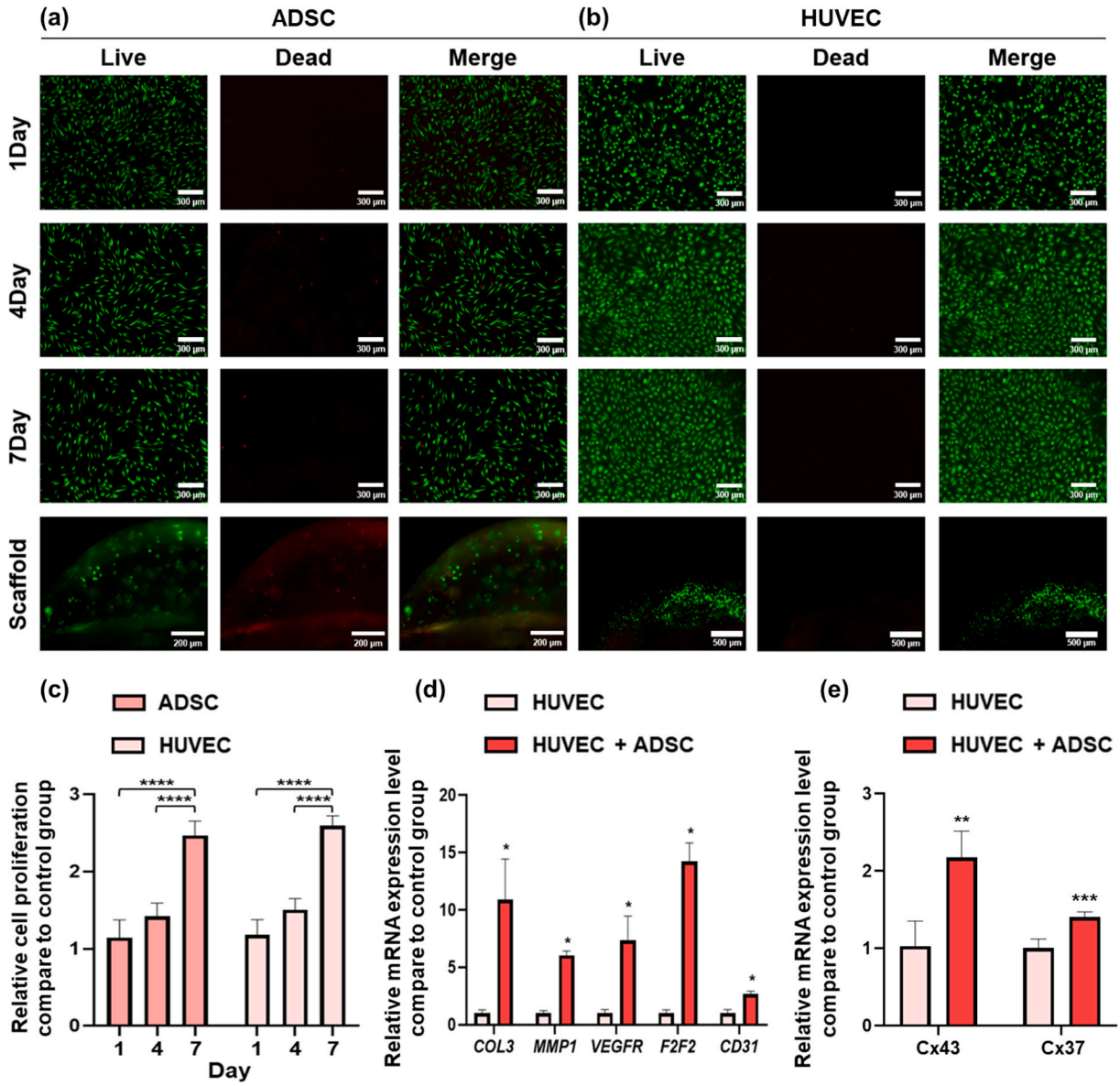

Fig. 2. Cytocompatibility evaluation of the tri-layer scaffold for wound regeneration. **(a)** Fluorescence micrographs of the live (green) and dead (red) cells in tri-layer scaffold elute and inside tri-layer scaffold in ADSC group. **(b)** Fluorescence micrographs of the live (green) and dead (red) cells in tri-layer scaffold elute and inside tri-layer scaffold in HUVEC group. **(c)** Cell proliferation test using ADSC, HUVEC cultured in tri-layer scaffold elutes (n = 3). **(d)** Quantitative expression of wound healing markers (Col3, MMP1), angiogenesis markers (VEGFR, FGF2, CD31), and **(e)** cell–cell interaction markers (Cx43, Cx37) in the tri-layer scaffold by qRT-PCR (day 3). The expression levels relative to the housekeeping gene (GAPDH) were calculated for analysis of qRT-PCR results (n = 3, * p-value < 0.05 versus the Day 1 group and HUVEC group). (For interpretation of the references to colour in this figure legend, the reader is referred to the web version of this article.)

VEGF signaling pathway in HUVECs (Fig. S4). Notably, such gene expression changes were not observed when the cells were cultured under conventional two-dimensional conditions, underscoring the importance of the 3D scaffold context in promoting vascularization-related gene expression.

Evaluation of wound recovery potential of HUVECs and ADSCs within tri-layer hydrogel scaffold

The wound-healing efficacy of the cell-laden tri-layer scaffold was first evaluated in vitro using a scratch wound assay with a transwell co-culture system. A schematic of the scratch assay setup is shown in Fig. 3a. After creating a scratch in a confluent monolayer of fibroblasts, different treatments were applied in the transwell insert above the wounded cell layer. In the control group (no treatment), the scratch showed minimal closure over 12 h (Fig. 3b), reflecting the limited inherent healing without intervention. A similar negligible improvement was observed when the tri-layer scaffold without cells was introduced, indicating that the scaffold alone did not significantly accelerate wound closure in this in vitro model.

In contrast, groups involving therapeutic cells demonstrated much faster wound closure. The addition of HUVECs (HUVEC + scaffold) led to appreciable scratch gap closure by 12 h, illustrating the beneficial effect of paracrine factors from endothelial cells on wound healing. More strikingly, when both ADSCs and HUVECs were combined within the scaffold (ADSC + HUVEC + scaffold), the wound gap exhibited substantial healing. By 24 h post-treatment, the co-culture scaffold group achieved nearly complete closure of the scratch wound, whereas other groups still showed considerable open area. Quantification of the wound closure over time supports these observations (Fig. 3c). The time-dependent recovery curves revealed that the co-culture scaffold group had the most rapid and extensive wound closure, significantly

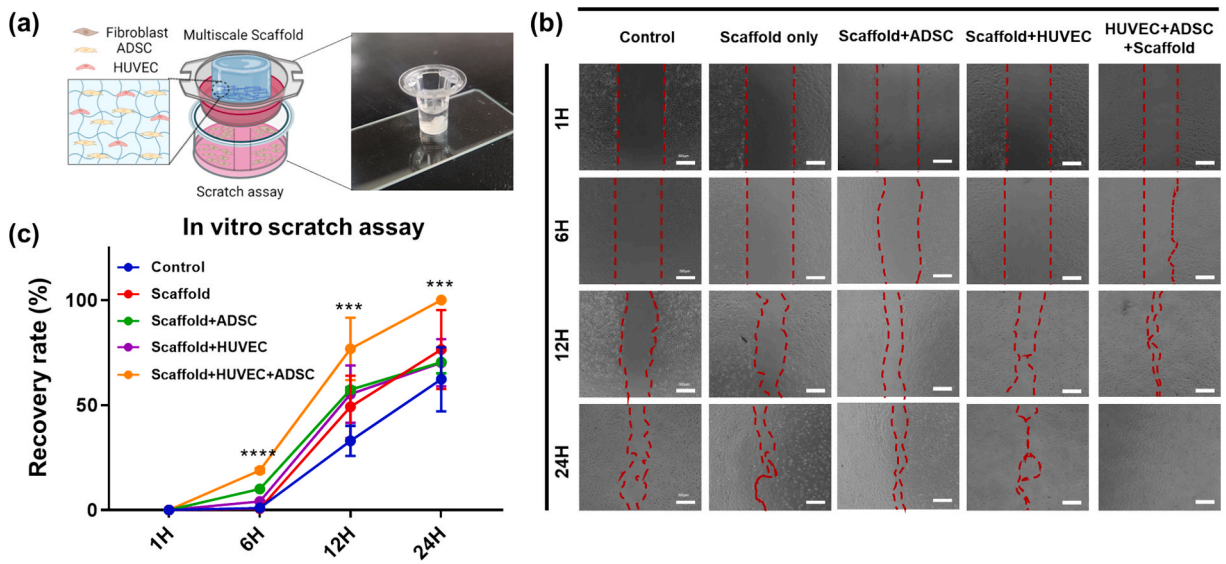

Fig. 3. Wound scratch assay of the tri-layer scaffold to evaluate wound recovery potential in vitro. **(a)** Schematic illustration of wound scratch assay with transwell and CCD camera image. **(b)** Representative microscope images of wound scratch assay to evaluate migration rates for 24 h with the tri-layer scaffold (Scale bar = 500 μm). **(c)** Quantitative analysis graph of in vitro scratch assay recovery rate of scaffold groups over time (n = 5, *** p-value < 0.001, **** p-value < 0.0001 versus the control group).

outperforming all other groups by 24 h ($p < 0.001$). These in vitro results demonstrate that integrating the tri-layer scaffold with both endothelial cells and stem cells creates a potent synergistic effect, greatly enhancing cell migration and wound closure in a simulated wound environment.

Improved wound healing effect of tri-layer cell-laden scaffold implanted in vivo model

The therapeutic potential of the tri-layer cell-laden scaffold was next tested in an in vivo wound model. Full-thickness skin wounds in mice were treated with various conditions and monitored for closure over 10 days. By day 10, wounds treated with the tri-layer hydrogel scaffold containing HUVECs and ADSCs showed dramatically improved healing compared to controls (Fig. 4a). These wounds contracted to roughly 10 % of their initial area, indicating nearly complete closure. In comparison, wounds covered with the scaffold alone (no cells) or with the two cell types applied without a scaffold (cell-only controls) still had ~ 20–45 % of the original wound area remaining open. Untreated wounds fared worst, with almost 40 % of the area unhealed on day 10. This outcome illustrates that the combination of the tri-layer scaffold with embedded regenerative cells accelerated wound contraction significantly more than either the scaffold or cells alone (or no treatment).

Histological analyses corroborated the superior healing observed in the cell-laden scaffold group. Hematoxylin and eosin (H&E) staining of wound cross-sections revealed complete re-epithelialization only in the HUVEC + ADSC + scaffold–treated wounds (Fig. 4b). In this group, a continuous, thick epidermal layer formed across the wound bed, bridging the defect and even slightly overlapping the wound edges, and the underlying dermis was relatively dense and well-organized. In contrast, the other groups showed only partial re-epithelialization: the new epidermis in those wounds was thin or discontinuous in the central area. These lesser-treated wounds also exhibited loosely organized granulation tissue in the dermal region, indicating delayed or incomplete healing compared to the fully treated group.

Collagen deposition patterns, visualized by Masson's trichrome staining, further highlighted differences in tissue regeneration among the groups (Fig. 4c). Wounds treated with the tri-layer hydrogel scaffold displayed a densely packed collagen matrix throughout the neodermis, approaching the richness and organization of normal skin. By contrast, wounds in the control, scaffold-only, and cell-only groups showed much sparser collagen in the wound bed, with thinner and disorganized collagen fibers indicative of a weaker, scar-prone repair tissue. The enhanced collagen deposition in the cell-seeded scaffold group suggests that the tri-layer construct provided an optimal environment for extracellular matrix production and remodeling, potentially leading to stronger, less scarred wound healing. Overall, the in vivo results demonstrate that the tri-layer scaffold, when loaded with regenerative cells, can substantially accelerate wound closure, promote orderly re-epithelialization, and guide collagen organization toward a more structurally robust and functionally integrated repair tissue.

Enhanced angiogenesis and dermal regeneration of tri-layer cell-laden scaffold implanted in vivo model

Immunofluorescence staining was used to evaluate neovascularization and skin maturation in the healed tissues. In wounds treated with the ADSC + HUVEC-laden scaffold, CD31-positive blood vessels were observed at high density throughout the wound bed (Fig. 5a). Quantitative image analysis showed that the CD31 fluorescence intensity in this group was roughly ten times greater than that in untreated wounds ($p < 0.01$). These CD31-labeled structures often presented as well-formed capillaries with open lumens, indicating robust angiogenesis within the regenerating tissue. By contrast, control wounds exhibited only sparse CD31 signals, reflecting minimal new vessel formation.

Laminin staining provided insight into basement membrane restoration during healing (Fig. 5b). In the cell-laden scaffold group, laminin was abundantly deposited as a near-continuous band along the wound interface, effectively re-establishing an intact basement membrane under the new epidermis. The laminin signal in these treated wounds was more than ten-fold higher than in untreated controls ($p < 0.01$). In stark comparison, control groups showed only fragmented and patchy laminin deposition, signifying incomplete or delayed basement membrane formation across the wound area.

Epidermal differentiation was assessed by involucrin expression (Fig. 5c). Wounds treated with the HUVEC + ADSC scaffold displayed strong, uniform involucrin staining in the suprabasal layers of the neoepidermis, indicative of a well-formed, stratified epidermis. The involucrin intensity in the treated group was approximately 12-fold higher

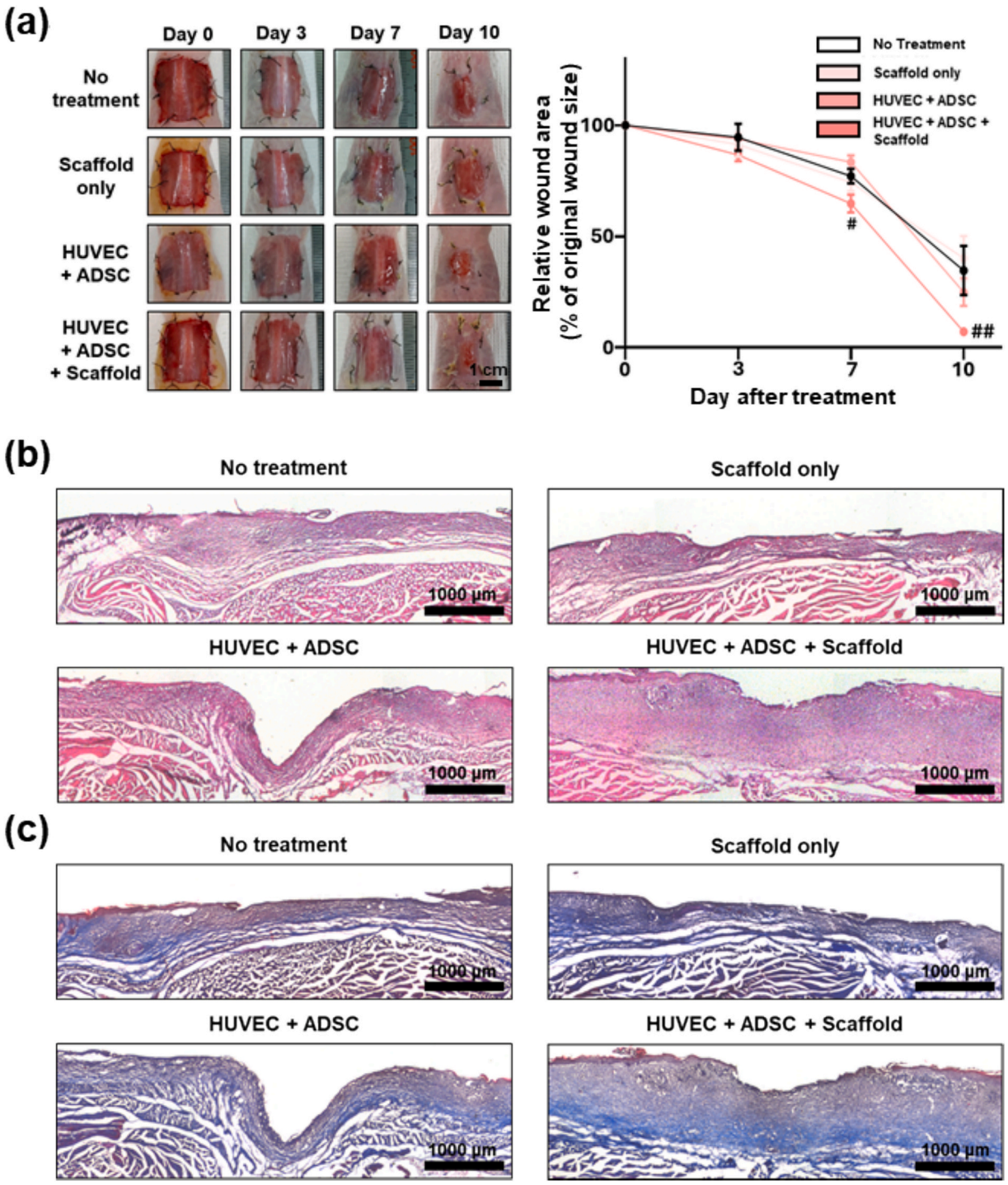

Fig. 4. Improved wound repair effect 10 days after surgery. **(a)** Macroscopic images of the wound sites with corresponding closure percentages (n = 4, # $p < 0.05$, ## $p < 0.01$ versus all other groups). **(b)** Hematoxylin and eosin stained sections and **(c)** Masson's trichrome stained sections collected on day 10, illustrating re-epithelialization and collagen deposition, respectively (Scale bar = 1000 μm).

than that of untreated wounds ($p < 0.001$). In the absence of the cell-laden scaffold, involucrin signals were faint and discontinuous, suggesting that epidermal maturation remained poor in those cases. Together, these results confirm that the tri-layer scaffold loaded with ADSCs and HUVECs not only accelerates the rate of wound closure but also significantly improves the quality of the regenerated tissue. The fully cell-seeded scaffold simultaneously enhanced vascularization, facilitated proper dermal architecture, and supported the formation of a mature epidermis, outcomes that were not achieved in control wounds.

Discussion

Our results demonstrate that integrating PCL fibers and an alginate outer layer with a fibrin hydrogel yields a scaffold with synergistically enhanced properties for wound healing [26]. This tri-layer design effectively balances flexibility and mechanical robustness, which is crucial for biomaterial scaffolds in the dynamic environment of a wound bed [31]. Notably, the composite scaffold's stiffness, with a Young's modulus of approximately 30 kPa, falls within the optimal range repeatedly reported for wound-healing hydrogels, being neither too

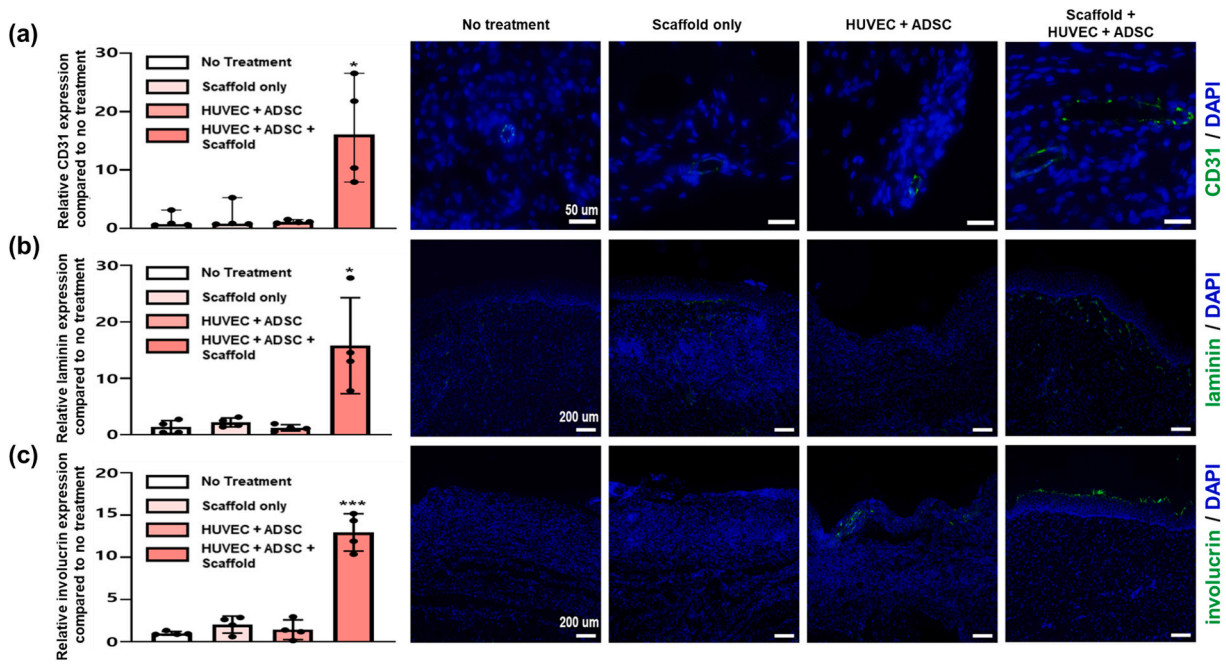

Fig. 5. Enhanced angiogenesis and dermal regeneration at 10 days post-surgery. **(a)** Quantitative expression and immunohistological images of microvessel marker (CD31, scale bar = 50 μm, n = 4, blue: nucleus, green: CD31). **(b)** Quantitative expression and immunohistological images of dermis marker (laminin, scale bar = 200 μm, n = 4, blue: nucleus, green: laminin). **(c)** Quantitative expression and immunohistological images of epidermis marker (involucrin, scale bar = 200 μm, n = 4, blue: nucleus, green: involucrin. *$p < 0.05$, ***$p < 0.001$ compared to no treatment group. (For interpretation of the references to colour in this figure legend, the reader is referred to the web version of this article.)

rigid to hinder tissue remodeling nor too soft to lose shape under physiological stress [32,33]. The incorporation of alginate contributed significantly to the scaffold's mechanical stability, as evidenced by the higher storage modulus and tensile strength of the tri-layer construct compared to fibrin or fibrin + PCL formulations [34]. Moreover, the tri-layer scaffold's high swelling capacity, which allows it to absorb over 1000 % of its weight in fluid, is a key advantage. This enables it to effectively soak up wound exudate and maintain a moist environment at the injury site [35]. A properly moist wound bed is known to accelerate healing by facilitating cell migration and extracellular matrix deposition, so this property directly contributes to the scaffold's therapeutic efficacy.

In addition to these physical properties, the tri-layer scaffold proved to be highly biocompatible, supporting the survival and proliferation of the encapsulated ADSCs and HUVECs. Co-culturing these two cell types in the scaffold not only maintained their viability but also enhanced their regenerative activity. We observed significant upregulation of wound-healing genes (such as COL3A1 and MMP1) and angiogenic factors (VEGFR, FGF2, CD31) in the HUVEC + ADSC co-culture, indicating that the 3D scaffold environment induced a coordinated response of extracellular matrix remodeling and new vessel formation [18,36,37]. One explanation for this enhanced activity is that the tri-layer architecture provides a mild hypoxic niche, as evidenced by elevated HIF-1α levels in 3D-cultured cells, which in turn triggers the HIF-1α/VEGF signaling pathway [38]. Notably, such robust gene activation was not seen in standard 2D cultures, highlighting how the three-dimensional microenvironment of the scaffold can unlock potent pro-angiogenic and pro-regenerative cellular responses.

A major factor in the improved healing observed with the ADSC + HUVEC-laden scaffold is the array of paracrine signals released by these cells. Mesenchymal stem cells and endothelial cells are known to secrete cytokines and growth factors such as SDF-1, VEGF, FGF, and HGF that recruit endogenous fibroblasts, immune cells, and progenitor cells to the wound site and stimulate their activity [39,40,41,42]. Likewise, factors like EGF, TGF-α, and CXCL12 (stromal cell-derived factor) help guide keratinocyte migration and proliferation, promoting faster re-epithelialization of the wound surface [43]. By providing a localized reservoir of these bioactive molecules, the cell-seeded tri-layer scaffold addresses the common issue of insufficient regenerative signaling in chronic or large wounds. However, as the scaffold gradually biodegrades over time, its structural integrity and ability to retain cells will diminish. Therefore, the enhancement in cell migration and tissue integration it provides is likely time-limited, with the most pronounced effects occurring in the early post-implantation period before the scaffold matrix significantly breaks down.

Our in vitro scratch-wound assay further highlighted the therapeutic potential of combining a biomaterial scaffold with regenerative cells. The rapid and nearly complete gap closure achieved by the co-cultured ADSC + HUVEC scaffold demonstrates that the tri-layer scaffold effectively delivers pro-migratory cues and enhances cell motility in a wound context [44,45]. This model simulates the cell migration phase of wound healing, and the superior performance of the cell-laden scaffold group provides clear evidence that the synergistic action of the two cell types within a supportive 3D matrix can significantly expedite the healing process.

Consistent with the in vitro findings, the in vivo wound healing outcomes were markedly improved by using the ADSC + HUVEC-seeded tri-layer hydrogel scaffold, in line with previously reported regenerative strategies that combine biomaterials with cells [46]. In treated wounds, not only was closure faster, but the quality of healing was also superior to controls, as we observed robust neovascularization, the formation of a continuous basement membrane, and a fully differentiated epidermis in the regenerated tissue. These results underscore the importance of addressing multiple facets of wound repair: the scaffold provides necessary structural support and maintains a moist and mildly hypoxic local environment, while the delivered cells supply growth factors and recruit host cells to orchestrate tissue regeneration in an organized manner. Such a combined approach clearly outperformed treatments employing the scaffold or cells alone, highlighting a synergistic effect that is greater than the sum of its parts in promoting effective wound

healing.

In summary, the tri-layer hydrogel scaffold particularly loaded with ADSCs and HUVECs offers a robust platform for enhancing wound healing, by modulating the wound microenvironment, promoting angiogenesis, and improving tissue regeneration. This design successfully balances mechanical strength and flexibility (preventing collapse while not hindering tissue movement), provides high absorbency for wound exudates, and creates a conducive 3D niche for cell survival and function. Compared to conventional single- or double-layer hydrogel dressings, our tri-layer approach integrates multiple beneficial features into one system, leading to significantly improved healing outcomes. The findings of this study suggest that engineering scaffolds to actively engage biological pathways through delivered cells and controlled microenvironment cues can dramatically advance regenerative medicine therapies. With further optimization, this tri-layer scaffold strategy could be adapted for chronic wounds or translated to other tissue engineering applications where expedited healing and tissue maturation are desired.

Conclusions

This study demonstrates that a tri-layer scaffold integrating PCL, fibrin, and alginate meets the key performance requirements for advanced wound dressings. The construction displays mechanical compliance appropriate for soft tissue, a high swelling capacity for exudate management, and excellent cytocompatibility, thereby delivering both structural support and a favorable cellular niche. In three-dimensional co-culture, the scaffold elevates the secretion of pro-regenerative paracrine factors, stimulating angiogenesis and matrix remodeling, which accelerates wound closure and produces more mature dermal and epidermal regeneration in vivo compared with conventional treatments. Owing to its tunable architecture, the tri-layer scaffold offers a versatile platform for wound care application, and it can be further customized by incorporating antimicrobial compounds or patient-specific cells to meet diverse clinical requirements in regenerative medicine.

CRediT authorship contribution statement

Yeong Hwan Kim: Writing – original draft, Methodology, Investigation, Data curation. **Gyubok Lee:** Writing – original draft, Methodology, Investigation, Data curation. **Dongwoo Kim:** Methodology, Formal analysis. **Young-Ju Jang:** Methodology, Formal analysis. **Sang Yoon Lee:** Methodology, Formal analysis. **Kangwon Lee:** Writing – original draft, Methodology, Formal analysis, Conceptualization. **Suk Ho Bhang:** Writing – original draft, Methodology, Formal analysis, Conceptualization.

Declaration of competing interest

The authors declare that they have no known competing financial interests or personal relationships that could have appeared to influence the work reported in this paper.

Acknowledgements

This research was supported by the Korean Fund for Regenerative Medicine funded by the Ministry of Science and ICT, Ministry of Health and Welfare (RS-2025-02213478, Republic of Korea). This work has been financially supported by Korean Fund for Regenerative Medicine (KFRM) grant funded by the Korea government (the Ministry of Science and ICT, the Ministry of Health & Welfare; project Number: 21A0102L1-12) and the KIST Institutional Program (Project No. 2E32351, 2E32350 “Development of cellular bloc platform technology”, Korea).

Ethical issues.

All animals received care according to the Guidelines for the Care and Use of Laboratory Animals of Sungkyunkwan University (SKKUIA-CUC2023-06-17-2, June 2023).

Appendix A. Supplementary data

Supplementary data to this article can be found online at https://doi.org/10.1016/j.jiec.2025.08.021.

Data availability

Data will be made available on request.

References

[1] G. McKnight, J. Shah, R. Hargest, Physiology of the skin, Surgery (Oxford) 40 (2022) 8–12.
[2] M. Čoma, J.C. Manning, H. Kaltner, P. Gál, The sweet side of wound healing: galectins as promising therapeutic targets in hemostasis, inflammation, proliferation, and maturation/remodeling, Expert Opin. Ther. Targets 27 (2023) 41–53.
[3] S. Ellis, E.J. Lin, D. Tartar, Immunology of wound healing, Curr Dermatology Rep. 7 (2018) 350–358.
[4] Wei X, Li M, Zheng Z, et al. Senescence in chronic wounds and potential targeted therapies. Burns & trauma. 10 (2022): tkab045.
[5] H.N. Wilkinson, M.J. Hardman, Senescence in wound repair: emerging strategies to target chronic healing wounds, Front. Cell Dev. Biol. 8 (2020) 773.
[6] M. Monami, B. Ragghianti, B. Nreu, V. Lorenzoni, M. Pozzan, A. Silverii, G. Turchetti, E. Mannucci, Major amputation in non-healing ulcers: outcomes and economic issues. Data from a cohort of patients with diabetic foot ulcers. the Int J of lower Extremity, Wounds 24 (2025) 235–244.
[7] P. Kujath, A. Michelsen, Wounds–from physiology to wound dressing, Dtsch. Arztebl. Int. 105 (2008) 239.
[8] Z.A. Obagi, G. Damiani, A. Grada, V. Falanga, Principles of wound dressings: a review, Surg. Technol. Int. 35 (2019) 57.
[9] Z. Ma, G. Bao, J. Li, Multifaceted design and emerging applications of tissue adhesives, Adv. Mater. 33 (2021) 2007663.
[10] M. Kohta, Y. Murooka, S. Soma, D. Ono, J. Sugama, H. Nemoto, Reducing effects of dressing materials on pressure and shear force for preventing heel pressure injury: an experimental study using three-axis tactile sensor, J Nurs Sci Eng. 9 (2022) 153–161.
[11] S.K. Stacey, M. McEleney, Topical corticosteroids: choice and application, Am. Fam. Physician 103 (2021) 337–343.
[12] I.R. Sweeney, M. Miraftab, G. Collyer, A critical review of modern and emerging absorbent dressings used to treat exuding wounds, Int. Wound J. 9 (2012) 601–612.
[13] B. Bhar, D. Chouhan, N. Pai, B.B. Mandal, Harnessing multifaceted next-generation technologies for improved skin wound healing, ACS Appl. Bio Mater. 4 (2021) 7738–7763.
[14] A. Nourian Dehkordi, F. Mirahmadi Babaheydari, M. Chehelgerdi, D.S. Raeisi, Skin tissue engineering: wound healing based on stem-cell-based therapeutic strategies, Stem Cell Res Ther 10 (2019) 1–20.
[15] Z. Si, X. Wang, C. Sun, Y. Kang, J. Xu, X. Wang, Y. Hui, Adipose-derived stem cells: sources, potency, and implications for regenerative therapies, Biomed. Pharmacother. 114 (2019) 108765.
[16] Y. Li, J. Long, Z. Zhang, W. Yin, Insights into the unique roles of dermal white adipose tissue (dWAT) in wound healing, Front. Physiol. 15 (2024) 1346612.
[17] Wang Y, Liu M, Zhang W, Liu H, Jin F, Mao S, Han C, Wang X. Mechanical strategies to promote vascularization for tissue engineering and regenerative medicine. Burns & Trauma. 12 (2024): tkae039.
[18] S. Rautiainen, T. Laaksonen, R. Koivuniemi, Angiogenic effects and crosstalk of adipose-derived mesenchymal stem/stromal cells and their extracellular vesicles with endothelial cells, Int. J. Mol. Sci. 22 (2021) 10890.
[19] F. Louis, Y. Sowa, S. Irie, Y. Higuchi, S. Kitano, O. Mazda, M. Matsusaki, Injectable Prevascularized Mature Adipose Tissues (iPAT) to Achieve Long-Term Survival in Soft Tissue Regeneration, Adv. Healthc. Mater. 11 (2022) 2201440.
[20] J. Gorecka, V. Kostiuk, A. Fereydooni, L. Gonzalez, J. Luo, B. Dash, T. Isaji, S. Ono, S. Liu, S.R. Lee, J. Xu, The potential and limitations of induced pluripotent stem cells to achieve wound healing, Stem Cell Res Ther 10 (2019) 1–10.
[21] I. Negut, G. Dorcioman, V. Grumezescu, Scaffolds for wound healing applications, Polymers 12 (2020) 2010.
[22] Y.Y. Li, S.F. Ji, X.B. Fu, Y.F. Jiang, X.Y. Sun, Biomaterial-based mechanical regulation facilitates scarless wound healing with functional skin appendage regeneration, Mil. Med. Res. 11 (2024) 13.
[23] A. Keirouz, M. Chung, J. Kwon, G. Fortunato, N. Radacsi, 2D and 3D electrospinning technologies for the fabrication of nanofibrous scaffolds for skin tissue engineering: a review, WIREs Nanomed. Nanobiotechnol. 12 (2020) e1626.
[24] H. Hall, Modified fibrin hydrogel matrices: both, 3D-scaffolds and local and controlled release systems to stimulate angiogenesis, Curr. Pharm. Des. 13 (2007) 3597–3607.
[25] D. Steiner, L. Lingens, L. Fischer, K. Köhn, R. Detsch, A.R. Boccaccini, T. Fey, P. Greil, C. Weis, J.P. Beier, R.E. Horch, Encapsulation of mesenchymal stem cells

improves vascularization of alginate-based scaffolds, Tissue Eng. Part A 24 (2018) 1320–1331.
[26] J. Ren, N. Kohli, V. Sharma, T. Shakouri, Z. Keskin-Erdogan, S. Saifzadeh, G. I. Brierly, J.C. Knowles, M.A. Woodruff, E. García-Gareta, Poly-ε-caprolactone/fibrin-alginate scaffold: a new pro-angiogenic composite biomaterial for the treatment of bone defects, Polymers 13 (2021) 3399.
[27] S. Pok, J.D. Myers, S.V. Madihally, J.G. Jacot, A multilayered scaffold of a chitosan and gelatin hydrogel supported by a PCL core for cardiac tissue engineering, Acta Biomater. 9 (2013) 5630–5642.
[28] K.C. Murphy, J. Whitehead, D. Zhou, et al., Engineering fibrin hydrogels to promote the wound healing potential of mesenchymal stem cell spheroids, Acta Biomater. 64 (2017) 176–186.
[29] M. Zhang, X. Zhao, Alginate hydrogel dressings for advanced wound management, Int. J. Biol. Macromol. 64 (2017) 176–186.
[30] C.R. Correia, S. Nadine, J.F. Mano, Cell encapsulation systems toward modular tissue regeneration: from immunoisolation to multifunctional devices, Adv. Funct. Mater. 30 (2020) 1908061.
[31] L. Tan, C. Huyan, Y. Wang, M. Li, D. Liu, M. Liu, Z. Luo, K. Cai, Y. Hu, Mechanically robust hemostatic hydrogel membranes with programmable strain-adaptive microdomain entanglement for wound treatment in dynamic tissues, ACS Nano 18 (2024) 8360–8382.
[32] M.H. Norahan, S.C. Pedroza-González, M.G. Sánchez-Salazar, M.M. Álvarez, G. T. de Santiago, Structural and biological engineering of 3D hydrogels for wound healing, Bioact. Mater. 24 (2023) 197–235.
[33] Z. Zeng, M. Zhu, L. Chen, Y. Zhang, T. Lu, Y. Deng, W. Ma, J. Xu, C. Huang, R. Xiong, Design the molecule structures to achieve functional advantages of hydrogel wound dressings: advances and strategies, Compos. Part B Eng. 247 (2022) 110313.
[34] A. Kumar, R.K. Mishra, K. Verma, S.M. Aldosari, C.K. Maity, S. Verma, R. Patel, V. K. Thakur, A comprehensive review of various biopolymer composites and their applications: from biocompatibility to self-healing, Mater Today Sustain. 23 (2023) 100431.
[35] D.V. Parikh, T. Fink, A.J. DeLucca, A.D. Parikh, Absorption and swelling characteristics of silver (I) antimicrobial wound dressings, Text. Res. J. 81 (2011) 494–503.
[36] V. Suresh, J.L. West, Adipose-derived stem cells can contribute to vascular network formation in poly (ethylene Glycol) hydrogel scaffolds, Regener. Eng. Transl. Med. 5 (2019) 180–189.
[37] L. Gan, P. Fagerholm, J. Palmblad, Vascular endothelial growth factor (VEGF) and its receptor VEGFR-2 in the regulation of corneal neovascularization and wound healing, Acta Ophthalmol. Scand. 82 (2004) 557–563.
[38] M. Ghahremani-Nasab, N. Akbari-Gharalari, A. Rahmani Del Bakhshayesh, A. Ghotaslou, A. Ebrahimi-Kalan, M. Mahdipour, A. Mehdipour, Synergistic effect of chitosan-alginate composite hydrogel enriched with ascorbic acid and alpha-tocopherol under hypoxic conditions on the behavior of mesenchymal stem cells for wound healing, Stem Cell Res Ther 14 (2023) 326.
[39] X.T. He, J. Wang, X. Li, Y. Yin, H.H. Sun, F.M. Chen, The critical role of cell homing in cytotherapeutics and regenerative medicine, Adv. Ther. 2 (2019) 1800098.
[40] D. Baltzis, I. Eleftheriadou, A. Veves, Pathogenesis and treatment of impaired wound healing in diabetes mellitus: new insights, Adv. Ther. 31 (2014) 817–836.
[41] R. Kosaraju, K.I. Bland, E. Roztocil, T.M. Crombleholme, S.G. Keswani, Adipose-derived stem cell-seeded hydrogels increase endogenous progenitor cell recruitment and neovascularization in wounds, Tissue Eng. Part A 22 (2016) 295–305.
[42] Y.J. Lin, G.H. Lee, C.W. Chou, Y.P. Chen, T.H. Wu, H.R. Lin, Stimulation of wound healing by PU/hydrogel composites containing fibroblast growth factor-2, J. Mater. Chem. B 3 (2015) 1931–1941.
[43] S. Lim, J.A. Kim, Y.H. Chun, H.J. Lee, Hyaluronic acid hydrogel for controlled release of heterobifunctional photocleavable linker-modified epidermal growth factor in wound healing, Int. J. Biol. Macromol. 253 (2023) 126603.
[44] Y. Sun, Y. Ju, B. Fang, Exosomes from human adipose-derived mesenchymal stromal/stem cells accelerate angiogenesis in wound healing: implication of the EGR-1/lncRNA-SENCR/DKC1/VEGF-A axis, Hum. Cell 35 (2022) 1375–1390.
[45] J.W. Wang, Y.Z. Zhu, J.Y. Ouyang, J.Y. Nie, Z.H. Wang, S. Wu, J.M. Yang, Y.Y. Yi, Adipose-derived stem cell extracellular vesicles improve wound closure and angiogenesis in diabetic mice, Plast. Reconstr. Surg. 151 (2023) 331–342.
[46] A.S. Klar, K. Michalak, S. Böttcher-Haberzeth, E. Reichmann, M. Meuli, T. Biedermann, The expression pattern of keratin 24 in tissue-engineered dermo-epidermal human skin substitutes in an in vivo model, Pediatr. Surg. Int. 34 (2018) 237–244.